Astron. Astrophys. 326, 318–328 (1997)

ASTRONOMY
AND
ASTROPHYSICS

A 200 km s^{-1} molecular wind in the peculiar carbon star V Hya

G.R. Knapp[1], **A. Jorissen**[1,⋆], **and K. Young**[2,⋆⋆]

[1] Department of Astrophysical Sciences, Princeton University, Princeton, NJ 08544, USA (gk@astro.princeton.edu, ajorisse@astro.ulb.ac.be)
[2] Caltech Submillimeter Observatory, P.O. Box 4339, Hilo, HI 96720, USA (rtm@dolson.harvard.edu)

Received 12 November 1996 / Accepted 1 April 1997

Abstract. A molecular wind with an outflow speed in excess of 200 km s^{-1} has been found in the AGB carbon star V Hya. Observations of several molecular lines show that the circumstellar envelope is expanding at 15 km s^{-1} and is flattened and inclined to the line of sight. The fast wind appears to be expanding from the poles of the envelope, with the expansion speed increasing with distance from the star. V Hya may be in the very earliest stage of evolution beyond the AGB.

Key words: stars: carbon – stars: individual – stars: mass-loss – stars: AGB and post-AGB

1. Introduction

On the basis of its properties at optical wavelengths, V Hya is usually considered to be a normal N type carbon star on the asymptotic giant branch (AGB). Its effective temperature is 2650 K, its spectral type is C6-7,5e and it is a semi-regular variable (SRa) with a period of 529 days (Kholopov et al. 1985; Lambert et al. 1986). The star has a large infrared excess and strong millimeter wavelength molecular line emission, showing that it is losing mass at a fairly high rate, several $\times$ 10^{-6} M$_\odot$ yr^{-1} (Zuckerman et al. 1977; Knapp & Morris 1985; Zuckerman & Dyck 1986; Tsuji et al. 1988; Kahane et al. 1988; Bujarrabal et al. 1994b,c; Stanek et al. 1995). The IRAS colors are also normal for carbon stars with high mass loss rates (cf. van der Veen & Habing 1988).

It has long been known from infrared and molecular line observations that the circumstellar envelope of V Hya is peculiar. The starlight is polarized at near infrared wavelengths, and both the degree of polarization and the position angle change with time, sometimes dramatically (Johnson & Jones 1991; Johnson 1993; Trammell et al. 1994). These observations show that the circumstellar envelope is not spherically symmetric, and that its density structure changes on timescales of months to years. The CO rotational line profiles differ from those seen in most carbon star envelopes; they have a double-horned structure and strong wings, and are considerably broader than lines from other molecular species in the envelope, such as CS and HCN (Bujarrabal et al. 1994b,c; Groenewegen et al. 1996; Knapp et al. in preparation.). Further, the emission at positive velocities with respect to the center of the line appears to arise from gas which is spatially separated from that emitting at negative velocities, suggesting that the outflow is bipolar (Tsuji et al. 1988; Kahane et al. 1988; Kahane et al. 1993, 1996, hereafter KABM). Recent high resolution observations of the stellar spectrum at optical and near infrared wavelengths show unusually broad absorption lines (Barnbaum et al. 1995). Absorption in the co v = 0–1 rotation-vibration line at 4.6μm extends to -130 km s^{-1} with respect to the stellar velocity (Sahai & Wannier 1988; Sugerman et al. 1997), while the optical spectrum shows forbidden-line emission reminiscent of that seen in Herbig-Haro objects, at a velocity blueshifted by 155 km s^{-1} with respect to the photospheric velocity (Lloyd Evans 1991). These data strongly suggest that V Hya is at an unusual evolutionary stage.

The observations described in the present paper were made to measure the CO millimeter-wavelength emission from V Hya with greater velocity resolution, sensitivity and velocity coverage than has been used for previous observations, to examine the emission line shapes and velocity widths, and to investigate the structure of the envelope. These observations discovered that the star has a molecular outflow with a speed $\geq$ 200 km s^{-1}. This paper describes this observation and its implications for AGB evolution. The next section discusses the molecular line observations and results and a kinematic model for the circumstellar envelope. Sect. 3 describes the broad-band spectrum of the star and models the infrared continuum emission and the molecular line emission to derive the mass loss rate and dust content of the envelope. Sect. 4 discusses the properties and evolutionary status of the star, and the conclusions are given in Sect. 5.

The basic data for V Hya from the literature are given in Table 1. The effective temperature, spectral type and abundances are from Lambert et al. (1986). The pulsation periods and variable type are from Mayall (1965) and Kholopov et al. (1985). V Hya is an N-type carbon star, and these objects in the Mag-

⋆ On leave from Institut d'Astronomie et d'Astrophysique, Université Libre de Bruxelles

⋆⋆ *Present address:* Harvard-Smithsonian Center for Astrophysics, 60 Garden St., Cambridge, MA 02138

Table 1. Basic data for V Hya

α(1950)	10 49 11.30
δ(1950)	–20 59 04.9
T_{eff}(K)	2650
D (pc)	380
R(cm)	2.9×10^{13}
L_{bol} ($L_\odot$)	7850
Sp. Type	N; C7,5
Var. Type	SRa
Period (days)	529.2 ($\Delta V = 1 - 1.5^m$)
	6275($\Delta V = 6^m$)

ellanic Clouds have an absolute K magnitude of -8.2^m (Cohen et al. 1981). The apparent K magnitude of -0.3^m (Bergeat et al. 1976) gives a distance of 380 pc. This distance estimate contains no correction for interstellar or circumstellar extinction. The resulting stellar luminosity and stellar radius are as derived by Luttermoser & Brown (1992).

2. Molecular Line Observations

The line observations were made in January 1996 using the 10.4 m telescope of the Caltech Submillimeter Observatory (CSO) on Mauna Kea, Hawaii. The telescope is equipped with SIS junction receivers cooled to liquid helium temperature. The observations were made of the CO(2–1) and CO(3–2) lines at 230 and 345 GHz and of CS and HC_3N lines at nearby frequencies. The atmospheric conditions were variable during the observing run, and the higher frequency observations were made during the better weather. The zenith atmospheric opacity at 225 GHz, measured by the NRAO tipping radiometer at the site, was between 0.1 and 0.15 for the 345 GHz observations and between 0.2 and 0.25 for the 230 GHz observations.

The frequencies of the observed spectral lines are given in Table 2. Three lines, CO(2–1), CS(5–4), and HC_3N(25–24) were observed in the 230 GHz band. The telescope half-power beamwidth was 30″, the main-beam efficiency was 76% and the single-sideband receiver temperature was $\sim$ 100 K. Two lines were observed in the 345 GHz band, CO(3-2) and CS(7-6). The telescope half-power beamwidth was 20″, the main beam efficiency 65%, and the receiver temperature $\sim$ 130 K. The effective single sideband system temperatures, including the effects of atmospheric emission and absorption, were $\sim$ 500 K at 230 GHz and $\sim$ 800 K at 345 GHz. The receivers for both bands are double-sideband, and spectral lines in the image sideband, 3 GHz below the observed frequency, are also detected.

The spectral lines were observed by three acousto-optic spectrographs (AOS) of which two at a time could be used. The first AOS has 2048 channels over a total bandwidth of 1.5 GHz, of which only the inner 1 GHz (the receiver bandwidth) produces usable data. The channel - to - channel spacing is $\sim$ 0.65 km s^{-1} and the resolution is $\sim$ 1.6 km s^{-1} at 345 GHz. The second has 1024 channels over a bandwidth of 500 MHz, giving a resolution of $\sim$ 1.2 km s^{-1} at 345 GHz and $\sim$ 1.6 km s^{-1} at 230 GHz. The third has 1024 channels over 50 MHz, giving a resolution of $\sim$ 0.12 km s^{-1} at 345 GHz and $\sim$ 0.2 km s^{-1} at 230 GHz. The spectrometer frequency was calibrated using an internally-generated frequency comb, and the velocity scale is corrected to the Local Standard of Rest (LSR).

The observations were made by chopping between the star position and an adjacent sky position with the secondary mirror. The chop throw was 120″ in azimuth at a rate of 1 Hz. Pairs of chopped observations were made with the source placed alternately in each beam. The spectral baselines resulting from this procedure are linear to within the r.m.s. noise. The CO emission from V Hya is strong enough that it can be used to measure the telescope pointing offsets, and the pointing was corrected every hour or so by mapping the integrated CO line flux from the star.

The temperature scale and the atmospheric opacity were measured by comparison with a hot (room temperature) load. The line temperature was corrected for the main beam efficiency, and the resulting scale is the Rayleigh-Jeans equivalent main beam brightness temperature T_{MB}, i.e. that measured by a perfect 10.4 m antenna above the atmosphere.

The remarkable new feature in V Hya revealed by these observations is a very fast molecular wind, seen as weak emission extending to about $\pm$165 km s^{-1} with respect to the velocity of the brighter CO emission. This weak emission is also seen in the CO(3–2) observations of V Hya. Such weak wings can be artificially produced in observations with acousto-optic spectrometers when they are slightly out of focus. We examined the shapes of the frequency calibration spikes; these show no detectable broad wings. Quantitatively, $T(V_c \pm 70$ km s$^{-1})/T(V_c)$ = 0.02 for both the CO(2–1) and CO(3–2) line observations, where V_c is the central velocity of the CO profile where the emission is brightest. The same quantity measured in the frequency comb spectra is $\leq$0.001. Further, no "wings" are seen on observations of the much stronger CO(3–2) and CO(2–1) emission from IRC+10216, which was also observed during this observing run. We are thus convinced of the reality of the fast wind from V Hya.

This fast wind has not been seen in the many observations of V Hya made previously, and its detection now can be attributed to the great improvements in sensitivity and baseline stability made possible by the new receivers and the chopping secondary mirror at the CSO. It can be identified with the high negative velocity CO 4.6 μm line absorption observed by Sahai & Wannier (1988) and Sugerman et al. (1997), the high velocity KI line absorption and fluorescent emission found by Plez & Lambert (1994), and the high negative velocity shocked-gas emission lines observed by Lloyd-Evans (1991). The CO(2–1) and, especially, the CO(3–2) observations (see below) show that this wind is symmetric in velocity and extends to higher velocities than observed previously. V Hya is thus one of the small group of evolved stars with molecular wind speeds in excess of 100 km s^{-1}.

The observational results are presented in Table 2 and Figs. 1–7. Table 2 lists the rest frequencies of the observed lines, the channel-to-channel r.m.s. noise (as measured by the 500 MHz AOS, except for the CO(3–2) and CS(7–6) lines, where

Table 2. Molecular line observations of V Hya

Line	Frequency (GHz)	r.m.s. (K)	Flux (K × km s^{-1})	T_{MB} (K)	V_c (km s^{-1})	V_e (km s^{-1})
CS (5 − 4)	244.936	0.012	2.52	0.13	−16.7	15.0
HC_3N (25 − 24)	227.419	0.010	0.82	0.06	−13.0	13.5
CS (7 − 6)	342.883	0.027	6.4	0.30	−18.8	15.2
CO (2 − 1)	230.538	0.010	45.8			
central component				1.5	-16	45
bipolar feature				–	–17	7
fast wind				0.04	–8	165
CO (3-2)	345.796	0.027	91.1			
central component				3.2	–14.6	47
bipolar feature					–16.6	8.2
fast wind				0.04	–20	200

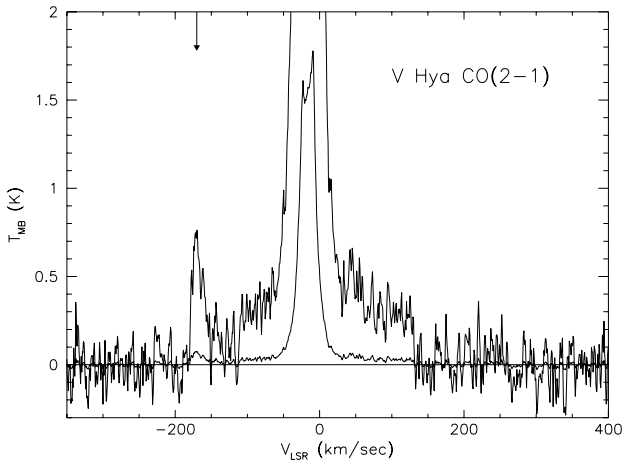

Fig. 1. CO(2-1) line profile observed at CSO. The abscissa is velocity with respect to the LSR and the ordinate the main-beam brightness temperature. The profile is shown twice: that drawn with the light line has the temperature scale expanded by a factor of 10. The line at "-170 km s^{-1}", indicated by the arrow, is the HC_3N(25-24) line in the image sideband.

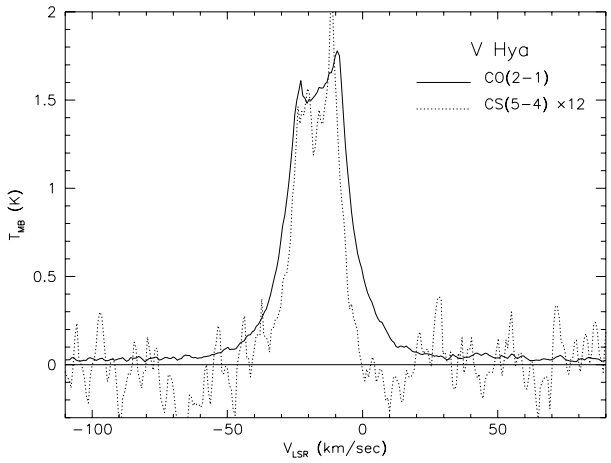

Fig. 2. The CS(5-4) line profile (dashed line) of V Hya compared with the central velocity portion of the CO(2-1) profile (solid line). The temperature scale is that for the CO(2-1) line, and the CS(5-4) scale has been expanded by a factor of 12.

the results from the 1.5 GHz AOS are used), the integrated line flux in units of K × km s^{-1}, the peak line temperature, the central velocity V_c and the terminal wind outflow speed V_e, which is measured from the half width of the line at zero intensity. The parameters for the CS and HC_3N lines were found by fitting parabolic profiles to the data (cf. Knapp & Morris 1985). The CO line shapes however are complex. Several components are identified in the profiles and are discussed below; the quantities listed in the last three columns of Table 2 are eye estimates.

The CO(2–1) line observed with the 500 MHz AOS is shown in Fig. 1. The feature at "−170 km s^{-1}" is the HC_3N(25–24) line at 227.4 GHz, detected in the image sideband. This line seems to have roughly the parabolic shape expected for spherical uniform outflow, and the parameters in Table 2 were found by fitting a parabola to the line profile after recalculating the velocity scale and removing the broad CO emission as a "baseline".

The CO line profile does not have the steep sided, roughly parabolic shape expected for uniform outflow; rather, its shape is roughly gaussian, and the line also shows asymmetric, double-peaked structure (Zuckerman & Dyck 1986; Kahane et al. 1988; Olofsson et al. 1988; Jura et al. 1988; Tsuji et al. 1988; Zuckerman & Dyck 1989; Nyman et al. 1992; Olofsson et al. 1993; Bieging & Latter 1994; Bujarrabal et al. 1994b,c; Stanek et al. 1995; KABM). The CO(2–1) line in Fig. 1 is considerably broader than the HC_3N line and has a full width at zero power, after removal of the broad CO emission, of $\sim$ 90 km s^{-1}, suggesting a wind outflow speed of $\sim$ 45 km s^{-1} (cf. KABM), much larger than the speed of $\sim$ 13.5 km s^{-1} given by the HC_3N line. The profile shape in Fig. 1 suggests that the 165 km s^{-1} and 45 km s^{-1} components are kinematically distinct.

Fig. 2 shows the CS(5–4) line profile compared with the CO(2–1) profile. The CS line is narrower than the CO line and

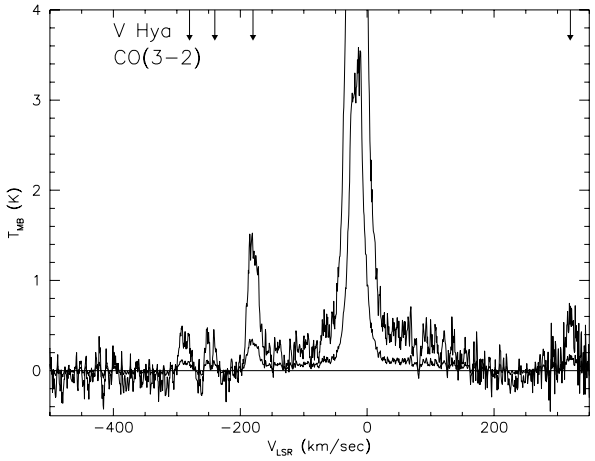

Fig. 3. The CO(3-2) line profile of V Hya. The light line shows the profile with the temperature scale expanded by a factor of 10. The line near "-180 km s^{-1}" is the CS(7-6) line in the image sideband, while that near "+320 km s^{-1}" is probably the $H^{13}CN$(4-3) line. The other two features between at "-240" and "-280" km s^{-1} are unidentified.

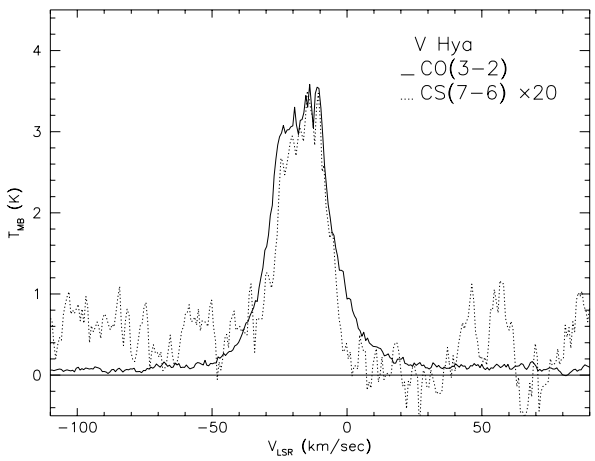

Fig. 4. The central part of the V Hya CO(3-2) line profile compared with that of the CS(7-6) line. The temperature scale of the CS(7-6) line is expanded by a factor of 20.

is double peaked; there is some suggestion that the velocities of the peaks relative to the star are smaller than are those of the CO peaks. There is no indication of the fast (165 km s^{-1}) wind in the CS profile, even when it is smoothed to a fairly coarse resolution, 10 km s^{-1}.

Fig. 3 shows the CO(3–2) line observed with the 1.5 GHz AOS. The excess noise beyond 250 km s^{-1} is due to the 1 GHz bandwidth. The feature at "-180 km s^{-1}" is the CS(7–6) line in the image sideband. That at "+320 km s^{-1}" is probably the $H^{13}CN$(4–3) line. The line shapes of the features at "-240 km s^{-1}" and "-280 km s^{-1}" suggest that these lines are in the image sideband; they show slight asymmetry which is the mirror image of the asymmetry seen in the CO line. We could find no plausible identification for them; they appear also in the spectrum of the bright carbon star IRC+10216. The CO(3–2) line has a very similar shape to the CO(2–1) line. The fast wind is even more pronounced at this frequency, and suggests an outflow speed of at least 200 km s^{-1}. Again, it seems to be kinematically distinct from the 45 km s^{-1} component. Fig. 4 shows the CS(7–6) line compared with the CO(3–2) line. The lines have similar shapes but the CS line is somewhat narrower and has steeper sides.

Observations of the CO(3–2) line were made at offsets of $\pm 20''$ (the full beamwidth) in right ascension and declination to investigate whether the envelope is significantly spatially extended. We did not attempt a fully sampled map; the IRAM telescope, with its $11''$ beam at 230 GHz, has made the best single-dish map currently available (KABM). Fig. 5a shows the CO(3–2) line profiles observed at $\pm 20''$ in declination, and Fig. 5b the profiles at $\pm 20''$ in right ascension.

The profiles observed north and south of the stellar position are roughly parabolic and centered on the stellar velocity. The difference in intensities may be due to spatial structure, but we cannot rule out the effect of small pointing errors. The expected

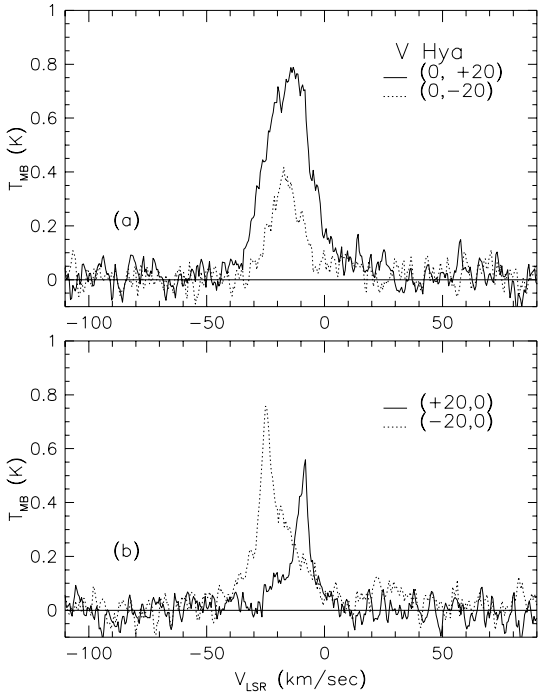

Fig. 5. a The CO(3-2) line profiles observed at $20''$ north and south of the central position of V Hya. **b** The CO(3-2) line profiles at $20''$ east and west of the central position of V Hya.

peak line temperature $20''$ from the center of V Hya is ~ 0.2 K if the molecular line emission is a point source on the scale of the CO(3–2) beam, compared with the observed values of 0.36 K at $20''$ south and 0.77 K at $20''$ north, showing that the envelope is slightly elongated in the north-south direction, in agreement with the results of KABM. The central velocity of the emission at both the north and south positions (~ -16 km s^{-1}) is roughly the same as that observed at the stellar position, and the line width is similar to that measured for the CS and HC_3N lines (Table 2).

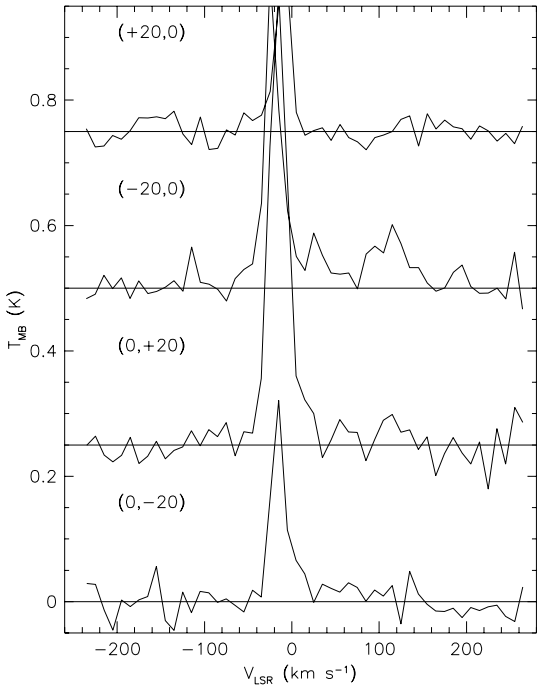

Fig. 6. CO(3–2) line profiles observed at positions offset from V Hya, smoothed to 10 km s^{-1} resolution.

By contrast, the line profiles observed at the right ascension offsets of $\pm 20''$ have quite different shapes. They show broad emission with a roughly parabolic shape at a peak strength T = 0.27 K $(-20'', 0)$ and T = 0.14 K $(+20'', 0)$, close to the values of 0.2 K expected if the CO emission in the envelope is a point source. In addition, these profiles have two sharp spikes, at velocities of -8.4 km s^{-1} at $+20''$ and -24.8 km s^{-1} at $-20''$. The mean velocity of these spikes is -16.6 km s^{-1}, very close to that measured from the CS and HC_3N lines, and their velocity difference is 16.4 km s^{-1}, giving an outflow speed of 8.2 km s^{-1}. Such line shapes cannot be produced by a spherical envelope expanding at constant velocity (cf. Fig. 5a); the spikes in Fig. 5b are almost certainly emitted by the same gas which produces the double-peaked shape of the CO(2–1) line (Fig. 1). The velocities of the peaks in the CO(2–1) line profile are -24 and -10 km s^{-1}, centered at -17 km s^{-1} and suggesting an outflow speed of $\sim$ 7 km s^{-1}.

Fig. 6 shows the CO(3–2) line profiles measured at the offset positions smoothed to a resolution of 10 km s^{-1}. The only profile showing believable high velocity emission is at $(-20'', 0)$, which may have weak emission to a velocity of about +130 km s^{-1} with respect to the star. There is a suggestion in the profiles at $(\pm 20'', 0)$ of fast bipolar emission, both for the 45 km s^{-1} wind and the 200 km s^{-1} wind, and that the bipolarity of the fast winds are in the opposite sense to that of the 8 km s^{-1} feature shown in Fig. 5b; i.e. the 8 km s^{-1} feature is at negative velocity at $(-20'', 0)$ while the faster winds are at positive velocity, and vice versa.

As these data show, V Hya's circumstellar molecular envelope does not have the simple geometry which seems to be the case (though less so as observations get better) for most envelopes, which are modeled reasonably well by a spherically symmetric wind expanding at constant velocity and mass loss rate. Rather, it appears as though several kinematic components, all centered at the stellar velocity, can be identified in the V Hya wind:

1) The "normal", slow wind. The outflow speed is difficult to determine from the CO line profiles alone. The CO(3–2) observations at $(0, \pm 20'')$ suggest $V_e = 22 - 25$ km s^{-1}; there may, however, be some contribution from faster-moving gas. The other molecular lines, CS(5–4), CS(7–6) and HC_3N(25–24), all give an outflow speed of about 15 km s^{-1}. We suggest that the "basic", "normal" red giant wind from V Hya can be identified with this 15 km s^{-1} outflow. The circumstellar envelope appears to be elongated in the north- south direction on a scale of $\sim 10'' - 15''$ (Fig. 5a; KABM).

2) The horns at ± 8 km s^{-1} (Fig. 1). These features arise from gas spatially separated by about $10''$ in the east-west direction (Fig. 5b) and are not prominent in the CO(3–2) line profile, which is observed with a smaller beam than is the CO(2–1) profile. The CO(2–1) map of KABM shows this spatial separation more clearly, and these authors point out that the profiles observed along the east-west axis have steep sides at ± 8 km s^{-1}, analogous to the steep sides of the line profiles from uniformly expanding spherical molecular winds. They propose that this component represents the outflow speed of the original circumstellar envelope produced by mass loss on the AGB, which has been sufficiently disrupted that it now contains only a small fraction of the envelope mass. This outflow speed is about half the value of 15 km s^{-1} suggested above.

3) The 45 km s^{-1} wind. This component has a shape which is more gaussian than parabolic and is considerably broader than the CS and HC_3N lines.

4) The 200 km s^{-1} molecular wind: this feature is seen in both the CO(2–1) and CO(3–2) lines, and is symmetric in velocity about the systemic velocity of the star. There is a slight suggestion in our mapping observations (Fig. 6) that this wind is bipolar. The bipolarity is shown much more clearly by the KI emission line observations of Plez & Lambert (1994), who find components at ± 130 km s^{-1} with respect to the stellar velocity, with a positional displacement between the positive and negative velocity gas of about $8''$.

Fig. 7 shows the ratio of the CO(3–2) and CO(2–1) intensities at the stellar position as a function of velocity. The data were averaged in bins of 10 km s^{-1}. The velocity ranges of the four wind components described above are shown. Fig. 7 shows that within the noise the line ratio at all velocities is close to the value of 2.25 expected if the CO(2–1) and CO(3–2) line emitting regions have the same brightness and same size and are smaller than the $20''$ CO(3–2) beam. The ratio is slightly smaller close to the line center, suggesting that the envelope is slightly resolved at $20''$, consistent with the discussion above.

The ratios of the total intensity and peak brightness temperature of the CS(7–6) and CS(5–4) lines, respectively 2.39 and 2.22, are also consistent with a molecular envelope with the bulk of its emission within the $20''$ telescope beam. Because the

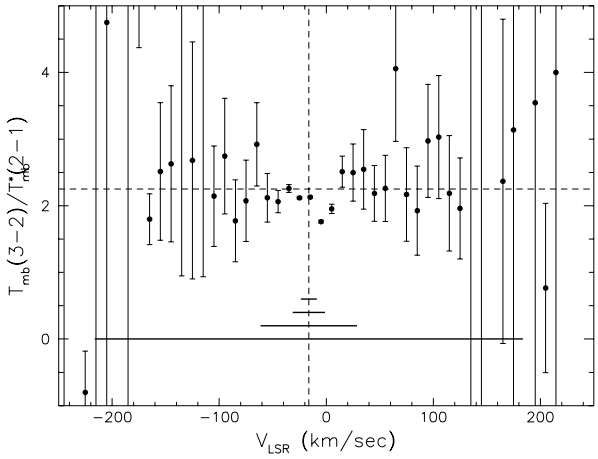

Fig. 7. Ratio of the intensities of the CO(3–2) and CO(2–1) lines at the stellar position from V Hya as a function of velocity. The vertical dotted line shows the mean velocity of the star. The horizontal dotted line shows the expected ratio for a source smaller than 20″. The heavy horizontal bars show the velocity ranges of the four components identified in the V Hya wind (see text).

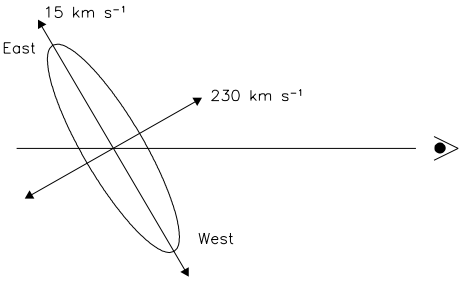

Fig. 8. Geometry of the V Hya circumstellar envelope. North is into the page.

emission from circumstellar molecular envelopes is centrally concentrated, the derivation of the angular size is not straightforward, but the present observations and those of KABM suggest that the envelope is only slightly extended and probably has an outer radius of 10″ or less. The IRAS observations of the circumstellar shell also find the envelope to be unresolved (Young et al. 1993a,b). At a distance of 380 pc, the linear radius of the envelope is only about 5×10^{16} cm and the envelope age, at an outflow speed of 15 km s^{-1}, is about 1000 years.

What is the underlying geometry? The mapping observations described by KABM and those in the present paper show that the CO emission near the systemic velocity (which we find from the measurements in Table 2 to be -16.3 km s^{-1}) is slightly elongated in the north-south direction. The outflow speed from the envelope, as given by the CS and HC_3N observations at the central position, and from the CO(3–2) lines observed 20″ north and south of the star, is about 15 km s^{-1}. The 4.6 μm absorption line observations by Sugerman et al. (1997) show a strong feature at -30 km s^{-1} with respect to the LSR which also provides evidence for an envelope outflow speed of 15 km s^{-1}. However, the CO(3–2) lines observed 20″ east and west of the center, and the CO(2–1) line observed at the central position, show strong narrow spikes at $\pm$8 km s^{-1}, which are spatially displaced from each other. Together, these observations suggest that the molecular outflow from V Hya has a velocity of 15 km s^{-1} but that it is in a flattened structure (sketched in Fig. 8) inclined to the line of sight, with the projected major axis lying approximately north-south. The $\pm$8 km s^{-1} spikes then arise from the gas along the minor axis, moving at 15 km s^{-1} and inclined at about 60^o to the line of sight. The CS and HC_3N lines arise from denser gas in the inner regions of the expanding disk, and so are not spatially resolved. This interpretation differs from that of KABM, who describe a model in which the basic envelope outflow is spherical with a velocity of 7.5 km s^{-1}, and with large cones gouged out by the fast winds.

We suggest that the most likely configuration for the high - velocity gas, both the strong 45 km s^{-1} wind and the weaker 200 km s^{-1} wind, is flow from the poles of the disk (Fig. 8). The evidence for this is admittedly sketchy, consisting of the mapping observations in Fig. 6 (where fast gas at positive velocities is tentatively seen in the profile at $(-20'', 0)$) and the optical emission line maps presented by Plez & Lambert (1994). If this model is correct, the fast gas is likely to have a space velocity of at least 230 km s^{-1}, and this star joins CRL 618 (Cernicharo et al. 1989; Gammie et al. 1989) and OH231.8+4.2 (Alcolea et alet al. 1996) in having a molecular outflow with velocity in excess of 200 km s^{-1}. The mapping observations in Fig. 6, and the line shapes, suggest that the outflow velocity increases with distance from the star. Perhaps the 200 km s^{-1} gas is moving freely, while the 45 km s^{-1} component is slow circumstellar gas swept up by the fast bipolar outflow. The fact that blue-shifted CO absorption is seen to about -130 km s^{-1} (Sugerman et al. 1997) suggests that the fast flow has a fairly large opening angle, so that much of the total velocity range is seen in absorption.

In summary, the observations described in this section suggest that V Hya is surrounded by a flattened molecular shell of radius $< 10^{17}$ cm expanding at $\sim$ 15 km s^{-1}. The star is also ejecting a fast molecular wind with at least two components, the first moving at about 50 km s^{-1} and the second at $\geq$ 230 km s^{-1}. Our observations provide very tentative evidence that the fast winds are bipolar and are flowing from the poles of the circumstellar shell, with speed increasing with distance from the star.

3. Circumstellar gas and dust

3.1. The mass of the circumstellar shell

The mass of circumstellar gas is now derived by modeling the CO observations. We assume a distance of 380 pc and a CO/H_2 ratio of 10^{-3}. The radius of the circumstellar shell was taken as 5×10^{16} cm, as given by the observations described in the previous section. As described above, the line profiles show that there are several kinematic components, and these were modeled separately - no attempt was made to construct a single model of the whole circumstellar shell. The line profiles for the 15 km s^{-1} component have a roughly parabolic shape

Table 3. Circumstellar envelope properties of V Hya

Component	M ($M_\odot$)	$\dot{M}$ ($M_\odot$ yr^{-1})	$T_{MB}(2-1)$ (K)	$T_{MB}(3-2)$ (K)	β	ϵ
Gas (15 km s^{-1})	2.2×10^{-3}	2.1×10^{-6}	1.0	2.0	0.2	0.005
Gas (45 km s^{-1})	5.2×10^{-3}	1.5×10^{-5}	0.6	0.9	3.9	0.10
Gas (200 km s^{-1})	5.8×10^{-4}	7.4×10^{-6}	0.04	0.08	8.7	0.22
Dust	2.1×10^{-5}	2.0×10^{-8}				

Notes: 1. Outer radius of 5×10^{16} cm assumed for all components 2. $\beta = \dot{M}\ V_e\ c/L_\star$ 3. $\epsilon = \dot{M}V_e^2/2L_\star$

(see especially Fig. 5a) and this component was modeled using the code described by Morris (1980) which assumes outflow at a constant speed and at constant mass loss rate, giving n(r) $\sim r^{-2}$. The 45 km s^{-1} and 200 km s^{-1} components do not have parabolic profiles, and were modeled using a constant-density LVG code based on that described by Goldsmith et al. (1983). Excitation both by collisions and by radiation at the 4.6 μm v = 0 $\rightarrow$ 1 transition of CO was included. The results are listed in Table 3, which gives for each component the total mass of gas within 5×10^{16} cm, the corresponding steady-state mass loss rate (the mass divided by the envelope crossing time), and the model main-beam brightness temperature at line center in the CO(2–1) and CO(3–2) lines as observed by a 10 meter telescope. We find, in agreement with KABM, that the 45 km s^{-1} component dominates the shell mass. The 200 km s^{-1} wind, however, dominates the shell energy and momentum. For all of these components, the radius of the CO emitting region were the shell to be truncated by photodestruction of CO (Mamon et al. 1988) is $1 - 1.5 \times 10^{17}$ cm, larger than the value of 5×10^{16} cm inferred from the CO mapping observations. Finally, Table 3 gives the ratios of the momentum and energy fluxes in each component relative to the corresponding quantities in the starlight. The momentum ratio in all cases is a lower limit, since the outflows are not isotropic.

The masses and in particular the mass loss rates in Table 3 are significantly higher than those derived by KABM, who find a total envelope mass of 2.1×10^{-3} $M_\odot$ and a total mass loss rate of 1.5×10^{-6} $M_\odot$ yr^{-1}. Ignoring the 200 km s^{-1} outflow which was not detected by KABM, our corresponding values are 5.3×10^{-3} $M_\odot$yr^{-1} and $\dot{M} = 1.2 \times 10^{-3}$ $M_\odot$ yr^{-1} (where we have used KABM's distance of 340 pc). The derived envelope masses agree to a factor of 2, and the large difference in the derived mass loss rate can be attributed to the smaller linear size for the V Hya envelope assumed in our calculations.

3.2. The circumstellar dust shell

The broad-band spectrum of V Hya, found using the data summarized in Table 4, is shown in Fig. 9. We used the data of Bergeat et al. (1976) & Noguchi et al. (1981) between 0.44 μm and 20 μm because both of these papers give data covering a broad wavelength range, and used the calibrations given in these papers to calculate the flux densities. The two papers have observations at J (1.25 μm) and H (1.65 μm) in common and the flux densities agree well (cf. Table 3) so it is reasonable to combine them. Other near infrared broad-band photometry for the star is given by Fouqué et al. (1992) and Kerschbaum & Hron (1994).

Table 4. Broad-band spectrum of V Hya

Wavelength	ν(GHz)	S_ν(Jy)	Ref
0.26μm	1.15×10^6	2.3×10^{-4}	1
0.32μm	9.38×10^5	6.8×10^{-3}	1
0.44μm	6.82×10^5	2.0×10^{-2}	2
0.55μm	5.45×10^5	1.6	2
1.00μm	3.00×10^5	216.4	3
1.25μm	2.4×10^5	348.6	2
1.25μm	2.4×10^5	372.1	3
1.65μm	1.82×10^5	856.6	2
1.65μm	1.82×10^5	802.0	3
2.2μm	1.36×10^5	1319.1	2
2.25μm	1.33×10^5	1107.5	3
2.3μm	1.30×10^5	1335.7	2
3.12μm	9.62×10^4	1046.9	3
3.5μm	8.57×10^4	2008.9	2
3.7μm	8.11×10^4	1531.8	3
4.8μm	6.25×10^4	1754.5	2
4.9μm	6.12×10^4	1788.3	2
8.4μm	3.57×10^4	2038.5	2
8.6μm	3.49×10^4	1632.8	2
10.8μm	2.78×10^4	1827.1	2
11.0μm	2.73×10^4	1911.6	2
12μm	2.5×10^4	1217.6	4
12.2μm	2.46×10^4	1570.9	2
18μm	1.67×10^4	673.1	2
20μm	1.50×10^4	513.0	2
25μm	1.2×10^4	469.3	4
60μm	5.0×10^3	109.15	4
100μm	3.0×10^3	29.92	4
1.1 mm	274.6	0.108	5
1.5 cm	20.0	$< 8.5 \times 10^{-3}$	6
3.6 cm	8.4	2.2×10^{-4}	7

1. IUE archival data
2. Bergeat et al. 1976
3. Noguchi et al. 1981
4. Co-added IRAS survey data
5. van der Veen et al. 1995
6. Sahai et al. 1989
7. Luttermoser & Brown 1992

The ultraviolet flux densities at 0.26 μm and 0.32 μm were measured from IUE archival data. The flux densities at 12 μm,

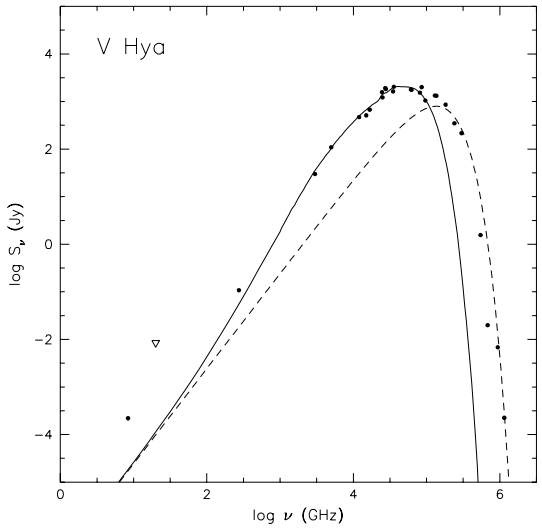

Fig. 9. Observed and model broad-band spectrum of V Hya. The open triangle is an upper limit. Dashed line: model black-body spectrum of star. Solid line: emission from star surrounded by dusty envelope (see text).

25 μm, 60 μm and 100 μm were obtained by co-adding the IRAS data and are in good agreement with the values in the IRAS Point Source Catalogue (1988). Finally, we list three observations at radio wavelengths from Sahai et al. 1989), Luttermoser & Brown (1992) and van der Veen et al. (1995).

Fig. 9 shows the results of two model curves fit to the data; the stellar flux, and the emergent flux from the model circumstellar dust shell (see below). The stellar emission was approximated as a black body with a luminosity of 7850 $L_\odot$, but the ultraviolet, optical and near-infrared flux densities suggest that the effective temperature of 2650 K derived by Lambert et al. (1986) may be a little high, and the model in Fig. 9 assumes $T_{\rm eff}$ = 2300 K. The IUE flux densities are consistent with this effective temperature and no extinction. This is in disagreement with the spectra measured by Lloyd-Evans (1991), who finds that V Hya has an excess of blue emission with respect to other cool variables and carbon stars, and shows Balmer absorption in the blue, suggestive of the presence of a blue companion. However, the radial velocity monitoring by Barnbaum et al. (1995) shows no evidence that V Hya is a spectroscopic binary, and the existence of a binary companion remains in question.

The radio frequency observations of V Hya are of considerable interest. The 20 GHz upper limit measured by Sahai et al. (1989) turns out to be too high to be useful, but the star is detected at 3.6 cm by Luttermoser & Brown (1992) in observations made in May-June 1989 and at 1.1 mm by van der Veen et al. (1995) in observations made about a year later. V Hya is the only star in the sample of carbon stars measured by Luttermoser & Brown from which radio continuum emission was detected, and its strength is well in excess of that expected from the stellar photosphere (cf. Fig. 9). The spectral index between 3.6 cm and 1.1 mm is 1.8$\pm$0.05, shallower than the black body value and almost certainly showing that the 3.6 cm emission is due to partly ionized gas near the star.

The broad-band spectrum of V Hya at wavelengths longer than about 3 μm was modeled by emission from circumstellar dust. We assumed a dust shell with n(r) $\sim$ r^{-2} consisting of spherical particles of amorphous carbon with radius 2000 Å and material density 1.85 gm cm^{-3}. Lorenz-Martins & Lefèvre (1994) show that such a model provides a reasonable fit to the spectrum of V Hya and derive a relative abundance of SiC to amorphous carbon of 3% from the strength of the 11.3 μm feature. Our model ignores this small amount of SiC and uses the optical constants for amorphous carbon calculated by Rouleau & Martin (1991). The longest wavelength (lowest frequency) for which these authors give data is 300 μm (10^3 GHz). The long wavelength emissivity Q_ν has a power-law dependence on frequency with index $\beta = 1$, and we estimated Q_ν at frequencies lower than 1000 GHz by extrapolation using this index.

The inner shell radius was set at the location where amorphous carbon evaporates or condenses, assumed to happen at 1500 K. The outer radius was the same as that used in modeling the CO emission. The resulting mass of dust and the corresponding dust loss rate (assuming an outflow speed of 15 km s^{-1}) are given in Table 3. The gas to dust ratio in the envelope is 360 by mass.

The model broad-band spectrum is compared with the data in Fig. 9, and fits the observations between 5 μm and 200 μm well. The model predicts far less flux at wavelengths shorter than 5 μm than is observed, showing that V Hya is not heavily obscured by circumstellar extinction, in agreement with the flattened geometry suggested by the CO data. Indeed, the broad-band spectrum in Fig. 9 could best be fit by the sum of the photospheric and dust shell emission. Many evolved stars with extensive circumstellar shells have similar broad-band spectra, and as Fig. 9 shows, their total fluxes may be overestimated by integrating the broad-band spectrum; the lack of spherical symmetry in the circumstellar envelope means that flux is contributed both by the relatively unobscured star and by the radiation from warm circumstellar dust when the structure is viewed close to pole-on. Derivation of the stellar bolometric flux in these cases needs a model of the circumstellar dust shell.

The other disagreement between the data and the model is at submillimeter and radio wavelengths. Both the observed 1.1 mm and, especially, the 3.6 cm flux density are well in excess of the predicted model flux density from both the stellar photosphere and the circumstellar dust. The models of van der Veen et al. (1995) show that the excess 1.1 mm emission cannot readily be explained by a second extended cold dust shell. Neither can the 3.6 cm flux; not only is the discrepancy much larger but the radio emission arises from a very small region; it is unresolved by the 2.25″ beam of the VLA, and so must arise from a region within 5×10^{15} cm of the star. Its likely source is ionized gas close to the star. Luttermoser & Brown (1992) suggest that the ionization is produced by shock propagation in the stellar chromosphere. Radio observations of several other cool evolved stars show similar excesses (Reid & Menten 1996; Knapp 1996; Reid & Menten 1997).

Table 5. Evolved stars with molecular wind velocities > 50 km s^{-1}

Star	V_e(km s^{-1})	Central Star	References	Bipolar?
CRL 618	19 190	B0	C89, G89, N92	y
OH 231.8 + 4.2	23 200	M6	M87, S95, A96	y
NGC 3132	26 55	A8V	S90	y
HD 101584	150	late B	L90, Y90, B96, K96	y
CPD $-$ 56°8032	16 59	WC	K96	?
BD + 30°3639	52	WC	B91	?
M1 $-$ 92	10 65	B0.5	B89, B94	y
CRL 2688	23 45 100	F8Iae	Y92, J92	y
V Hya	15 45 200	C7, 5		y

References: A96: Alcolea et al. 1996; B89: Bowers & Knapp 1989; B91: Bachillar et al. 1991; B94: Bujarrabal et al. 1994a; B96: Bakker et al. 1996c; C89: Cernicharo et al. 1989; G89: Gammie et al. 1989; K96: Knapp et al. in preparation; L90: Loup et al. 1990; M87: Morris et al. 1987; N92: Neri et al. 1992; S90: Sahai et al. 1990; S95: Stanek et al. 1995; T90: Trams et al. 1990; Y92: Young et al 1992; J92: Jaminet et al. 1992

4. Discussion

The molecular line observations of V Hya discussed in the previous section show that it is a member of an unusual group of evolved stars, those with very fast molecular winds. To date, eight evolved stars with molecular outflows at speeds exceeding 50 km s^{-1} are known. These are listed in Table 5, which gives the star name, the outflow speed(s) of the molecular wind(s), the spectral type of the central star, and references to molecular line data.

These stars have several other common properties. First, they are almost all evolved well past the AGB. CRL 618, NGC 3132, CPD $-$ 56°8032, M1-92 and BD + 30°3639 are planetary nebulae with hot nuclei, while HD 101584 and CRL 2688 have central stars much hotter than does the typical AGB star. Only OH 231.8+4.2, like V Hya, has a cool central star, of type M6-M9. A second common property among the stars in Table 5 is that almost all of the circumstellar envelopes have well-developed bipolar structure, and when sufficient resolution is used to make the molecular line observations, the winds themselves are also found to be bipolar (e.g. Bujarrabal et al. 1992, 1994a and references in Table 5).

The molecular line profiles for most of these stars show outflows at more than one velocity, as is the case for V Hya. Typically, the line profiles have a central component of roughly parabolic shape and width about 10 - 30 km s^{-1} and, centered at the same velocity, weaker, much broader line wings. Two of the stars in Table 5, HD 101584 and BD + 30°3639, show only the fast molecular wind. The mechanical luminosity (and momentum flux) of the fast wind is generally much larger than that of the slower wind, and can approach a significant fraction of the stellar luminosity (Table 3). It seems reasonable to identify the parabolic component with the wind shed while the star was on the AGB and to associate the fast wind with evolution beyond the AGB.

Fig. 10 shows the IRAS color-color diagram for V Hya and the stars in Table 5. The colors for CRL 2688, which is not in the IRAS Point Source Catalogue, were approximately found from photometry in the compilation by Gezari et al. (1993). V Hya is the only member of this group of objects with IRAS colors corresponding to those of AGB stars; the other stars all have very cold IRAS colors. Because the IRAS colors are those of very dense, hollow circumstellar shells, cold IRAS sources are considered to be highly evolved and indeed to be protoplanetary nebulae (not all cold IRAS sources have fast molecular winds, however; e.g. Likkel et al. 1987; Loup et al. 1990).

However, while V Hya's envelope appears to have IRAS colors like those of AGB stars, the lines of molecules like HCN,

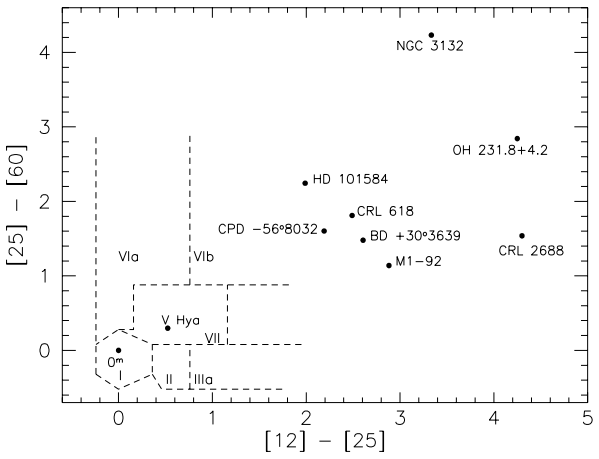

Fig. 10. IRAS color-color diagram for evolved stars with molecular wind speeds in excess of 50 km s^{-1}. The point labeled "0^m" corresponds to the colors of a zero magnitude infinite temperature black body. The dashed lines outline the region of the color-color diagram containing normal mass-losing carbon-rich and oxygen-rich AGB stars (van der Veen and Habing's 1988). Region I: photospheres, no circumstellar emission. Regions II and IIIa: oxygen rich envelopes. Region VII: carbon stars. Regions VIa and VIb: cool stars with detached shells.

CS and HC_3N, while present, are much weaker relative to the CO lines than in most carbon stars (Bujarrabal et al. 1994b,c). This chemistry resembles that of the CRL 618 envelope (Gammie et al. 1989). Since the emission from these species arises preferentially from the dense inner circumstellar envelope, the relative weakness of these molecular lines suggests that the inner region of V Hya's envelope is hollow due to the cessation of mass loss or the ionization/dissociation of the inner envelope.

As noted above, only V Hya and OH231.8+4.2 among the objects in Table 5 are cool stars. Like V Hya, OH231.8+4.2 has a Herbig-Haro like optical spectrum (Reipurth 1987), indicative of shock-induced emission, and this is probably due to the fast molecular wind colliding with the surrounding, more slowly moving circumstellar material. These comparisons, and Fig. 10, suggest that V Hya is at the very beginning phases of evolution away from the AGB.

V Hya is a member of a small class of doubly-periodic semi-regular variable stars (Lloyd Evans 1985, 1995), with variations of $1 - 1.5^{\rm m}$ amplitude and 529 day period superimposed on variations with a much larger amplitude ($\sim 6^{\rm m}$) and longer-period (17 - 18 years, Mayall 1965). The deep minima are much weaker at longer wavelengths. Moreover, Johnson (1993) reports a strong increase in the V-band polarization from 0.7% to 10% at the time of the optical fading. Lloyd Evans (1993, 1995) suggests that the deep minima are associated with episodes of dust formation, such as those seen in Type b RV Tau variables. These doubly-periodic stars are believed to have started to cross the HR diagram, and their relationship with post-AGB stars has been discussed by Gingold (1986), Bujarrabal et al. (1990), and Lloyd-Evans (1995).

V Hya has the broadest photospheric absorption lines in a large sample of carbon stars measured by Barnbaum et al. (1995). These authors suggest that the line is rotationally broadened, due to envelope spin-up during a short-lived common envelope binary phase. However, such broad lines are a distinctive property of post-AGB stars (e.g. Bakker et al. 1996a,b), with macroturbulence considered to be the main broadening mechanism (Gray 1992).

Thus, the photometric, polarization, spectroscopic and circumstellar envelope features of V Hya are not unusual when compared with those of post-AGB stars and protoplanetary nebulae. However, V Hya is unusual in this group of stars in having a low effective temperature and IRAS colors like those of AGB stars. It may therefore represent the earliest phase of evolution beyond the AGB yet found.

If this is so, the presence of a very fast molecular wind in V Hya's envelope shows that this phenomenon takes place immediately upon entering the post-AGB phase of evolution and may, to all intents and purposes, initiate it. The low mass and short dynamical time (1000 years) of the circumstellar envelope suggest that evolution away from the AGB is also accompanied by a short period of copious mass loss. The mechanism causing fast bipolar molecular winds in single stars is not obvious, though it may imply the dumping of large amounts of energy into the stellar envelope as the star moves away from the AGB.

In conclusion, the body of observational data for V Hya indicates that it is at an unusual and short-lived evolutionary phase. If it is just beginning its evolution away from the AGB, as the observations suggest, the molecular line observations show that the fast, powerful molecular winds which are present in several post-AGB stars are initiated at the very beginning of post-AGB evolution.

5. Conclusions

1. Molecular line observations of the carbon star V Hya show that there are three wind components in its circumstellar shell, flowing at speeds of 15, 45 and 200 km s^{-1}.
2. V Hya is the first star still on the AGB found to be producing a very fast molecular wind.
3. Most of the mass of the circumstellar envelope is in the 45 km s^{-1} component, but most of the energy is in the 200 km s^{-1} wind.
4. The envelope is slightly resolved. The horns on the CO line profiles at ± 8 km s^{-1} are the result of resolution and are spatially separated. The simplest geometry which explains the observed molecular line profiles is a flattened disk expanding at 15 km s^{-1}, inclined to the line of sight, from whose poles the faster molecular winds are flowing.

Acknowledgements. We would like to thank the referee, Hans Olofsson, for very useful comments, and Mark Morris, Cecilia Barnbaum and Claudia Kahane for sending us papers in advance of publication. We thank the staff at CSO, especially Antony Schinkel, Maren Purves and Tom Phillips, for their help with the observations. Astronomical research at the CSO is supported by the National Science Foundation via grant AST93-13929. This research made use of the SIMBAD data base, operated at CDS, Strasbourg, France. Support for this work

from Princeton University and Fonds National de la Recherce Scientific (Belgium) is gratefully acknowledged. AJ is Research Associate with F.N.R.S. (Belgium).

References

Alcolea, J., Bujarrabal, V., Sánchez Contreras, C. 1996, A&A, 312, 560
Bachillar, R., Huggins, P.J., Cox, P., Forveille, T. 1991, A&A 247, 525
Bakker, E.J., van der Wolf, F.L.A., Lamers, H.J.G.L.M., et al. 1996a, A&A 306, 924
Bakker, E.J., Lamers, H.J.G.L.M., Waters, L.B.F.M., et al., 1996b, A&A 307, 869
Bakker, E.J., Lamers, H.J.G.L.M., Waters, L.B.F.M., Waelkens, C. 1996c, A&A 310, 861
Barnbaum, C., Morris, M., Kahane, C. 1995, ApJ 450, 862
Bergeat, J., Sibille, F., Lunel, M., Lefèvre, J. 1976, A&A 52, 227
Bieging, J.H., Latter, W.B. 1994, ApJ 422, 765
Bowers, P.F., Knapp, G.R. 1989, ApJ 99, 476
Bujarrabal, V., Alcolea, J., Bachillar, R. 1990, A&A 234, 355
Bujarrabal, V., Alcolea, J., Neri, R., Grewing, M. 1994, ApJ 436, L169
Bujarrabal, V., Alcolea, J., Planesas, P. 1992, A&A 257, 701
Bujarrabal, V., Fuente, A., Omont, A. 1994a, ApJ 421, L47
Bujarrabal, V., Fuente, A., Omont, A. 1994b, A&A 285, 247
Cernicharo, J., Guélin, M., Martin-Pintado, J., Peñalver, J., Mauersberger, R. 1989, A&A 222, L1
Cohen, J.G., Frogel, J.A., Persson, S.E., Elias, J.H. 1981, ApJ 249, 481
Fouqué, P., Le Bertre, T., Epchtein, N., Guglielmo, F., Kerschbaum, F. 1992, A&AS 93, 151
Gammie, C.F., Knapp, G.R., Young, K., Phillips, T.G., Falgarone, E. 1989, ApJL 345, L87
Gezari, D.Y., Schmitz, M., Pitts, P.S., Mead, J.M. 1993, 'Catalogue of Infrared Observations', NASA Ref. Pub. 1294
Gingold, R.A. 1986, Mem. Soc. Astron. It. 56, 169
Goldsmith, P.F., Young, J.S., Langer, W.D. 1983, ApJS 51, 203
Gray, D.F. 1992, "The Observation and Analysis of Stellar Photospheres", Cambridge University Press
Groenewegen, M. A. T., Baas, F., de Jong, T., Loup, C. 1996, A&A 306, 241
IRAS Point Source Catalogue, 2nd Edition, 1988, NASA Reference Publications, Washington DC.
Jaminet, P.A., Danchi, W.C., Sandell, G., Sutton, E.C. 1992, ApJ 400, 513
Johnson, J.J. 1993, BAAS 25, 1423
Johnson, J.J., Jones, T.J. 1991, AJ 101, 1735
Jura, M., Kahane, C., Omont, A. 1988, A&A 201, 80
Kahane, C., Audinos, P., Barnbaum, C., Morris, M. 1993, in 'Mass Loss on the AGB and Beyond', ed. H. Schwarz, ESO Conference and Workshop Proceedings # 46, p437 (KABM)
Kahane, C., Audinos, P., Barnbaum, C., Morris, M. 1996, A&A 314, 871 (KABM)
Kahane, C., Maizels, C., Jura, M. 1988, ApJ 328, L25
Kerschbaum, F., Hron, J. 1994, A&AS 106, 397
Kholopov, P.N., Samus, N.N., Frolov, M.S., et al 1985, 'General Catalogue of Variable Stars', Moscow, Nauka Publishing House, Vols 1-4
Knapp, G.R. 1996, in 'Radio Emission from the Stars and the Sun", ed. A.R. Taylor and J. M. Parades, ASP Conference Series 93, 71
Knapp, G.R., Morris, M. 1985, ApJ 292, 640
Lambert, D. L., Gustafsson, B., Eriksson, K., Hinkle, K. H. 1986, ApJS 62, 373
Likkel, L., Omont, A., Morris, M., Forveille, T. 1987, A&A 173, L11
Lloyd Evans, T. 1985, MNRAS 217, 493
Lloyd Evans, T. 1991, MNRAS 248, 479
Lloyd Evans, T. 1993, IAU Circ 5852
Lloyd Evans, T. 1995, Ap. Space Sci. 230, 169
Lorenz-Martins, S., Lefèvre, J. 1994, A&A 291, 831
Loup, C., Forveille, T., Nyman, L.A., Omont, A. 1990, A&A 227, L29
Luttermoser, D.G., Brown, A. 1992, ApJ 384, 634
Mamon, G.A., Glassgold, A.E., Huggins, P.J. 1988, ApJ 328, 797
Mayall, M. W. 1965, JRASC 59, 245
Morris, M. 1980, ApJ 236, 823
Morris, M., Guilloteau, S., Lucas, R., Omont, A. 1987, ApJ 321, 888
Neri, R., Garcia-Burillo, S., Guelin, M., et al. 1992, A&A 262, 544
Noguchi, K., Kawara, K., Kobayashi, Y., Okuda, H., Sato, S. 1981, PASJ 33, 373-97
Nyman, L.A., Booth, R.S., Carlström, U., et al. 1992, A&AS 93, 121
Olofsson, H., Eriksson, K., Gustafson, B. 1988 A&A, 196, L1
Olofsson, H., Eriksson, K., Gustafsson, B., Carlström, U. 1993, ApJS 87, 305
Plez, B., Lambert, D.L. 1994, ApJ 425, L101
Reid, M.J., Menten, K.M. 1996, in 'Radio Emission from the Stars and the Sun', ed. A.R. Taylor and J. M. Parades, ASP Conference Series 93, 71
Reid, M.J., Menten, K.M. 1997, ApJ 476, 327
Reipurth, B. 1987, Nature 325, 787
Rouleau, F., Martin, P.G. 1991, ApJ 377, 526
Sahai, R., Claussen, M.J., Masson, C.R. 1989, A&A 220, 92
Sahai, R., Wannier, P.G. 1988, A&A 201, L9
Sahai, R., Wootten, A., Clegg, R.E.S. 1990, A&A 234, L1
Stanek, K.Z., Knapp, G.R., Young, K., Phillips, T.G. 1995, ApJS 100, 169
Sugerman, B., Sahai, R., Hinkle, K. 1997, in I.A.U. Symposium 170 "CO: Twenty-Five Years of Millimeter Wave Spectroscopy", ed. J. Bally, Kluwer Scientific, in press.
Trammell, S.R., Dinerstein, H.L., Goodrich, R.W. 1994, AJ 108, 984
Trams, N.R., van der Veen, W.E.C.J., Waelkens, C., Waters, L.B.F.M., Lamers, H.J.G.L.M. 1990, A&A 233, 153
Tsuji, T., Unno, W., Kaifu, N., et al. 1988, ApJ 327, L23
van der Veen, W.E.C.J., Habing, H.J. 1988, A&A 194, 125
van der Veen, W.E.C.J., Omont, A., Habing, H.J., Matthews, H.E. 1995, A&A 295, 445
Young, K., Phillips, T.G., Knapp, G.R. 1993a, ApJS 86, 517
Young, K., Phillips, T.G., Knapp, G.R. 1993b, ApJ 409, 725
Young, K., Serabyn, G., Phillips, T.G., et al. 1992, ApJ 385, 265
Zuckerman, B., Dyck, H.M. 1986, ApJ 311, 345
Zuckerman, B., Dyck, H.M. 1989, A&A 209, 119
Zuckerman, B., Palmer, P., Morris, M., et al. ApJ 211, L97